Excitation and detection of high-frequency coherent acoustic phonons in low-symmetry superlattices

P. Walker, R. P. Campion, and A. J. Kent
School of Physics and Astronomy, University of Nottingham, Nottingham NG7 2RD, United Kingdom

D. Lehmann
Institute of Theoretical Physics, Technische Universität Dresden, D-01062 Dresden, Germany

Cz. Jasiukiewicz
Faculty of Mathematics and Applied Physics, Rzeszow University of Technology, ul. W. Pola 2, PL-35-959 Rzeszow, Poland
(Received 11 July 2008; published 10 December 2008)

The generation and detection of coherent acoustic phonons in GaAs/AlAs superlattices grown on the low-symmetry, (311) and (211), planes of GaAs using femtosecond time-resolved pump-probe measurements is described. Frequencies of the excited phonons are deduced from the oscillations in the surface reflectivity of the probe and are compared with theoretical calculations assuming that Raman scattering is responsible for coherent phonon generation. The measured frequencies and relative intensities of the modes agree well with the theoretically predicted folded bulk acoustic modes and are determined by the period and symmetry of the superlattices.

DOI: 10.1103/PhysRevB.78.233307 PACS number(s): 63.20.D−, 63.22.Np, 68.65.Cd

Recently, there has been considerable interest in developing usable sources of monochromatic acoustic phonon beams in the terahertz range for applications in phonon spectroscopy of nanostructures and high-speed optical modulation. Generation of high intensity pulses of zone-folded longitudinally polarized (LA) coherent acoustic phonons in GaAs/AlAs superlattices (SLs) by ultrafast optical excitation has been demonstrated by a number of groups, see, e.g., Refs. 1 and 2. The frequency of the phonons is determined by the SL period, d_{SL}, and is given approximately by c_s/d_{SL}, where c_s is the velocity of sound in the SL. It has also been shown that the phonons leak out of the superlattice and propagate over macroscopic distances at low temperature,[3] which is important for the potential applications mentioned above. However, most work was restricted to SLs grown on (100) GaAs.

Superlattices grown on the low-symmetry, e.g., (311) and (211), planes of GaAs allow the possibility of generating also coherent transverse polarized (TA) acoustic phonon modes using femtosecond excitation.[4] No such possibility exists for (100) SLs due to symmetry considerations. However, owing to the low symmetry, TA modes are Raman active in (311) and (211) SLs as has been shown in Raman-scattering measurements,[5,6] and this could facilitate their generation and/or detection in femtosecond pump-probe measurements.

The aim of the work described here was to obtain a more complete theoretical model of the processes of generation and detection of coherent acoustic phonons in low-symmetry SLs by femtosecond optical techniques. This is necessary because the results of conventional Raman-scattering measurements and associated theoretical models may not be directly applicable to resonant optical excitation by femtosecond pulses. Furthermore, standard Raman-scattering measurements normally probe the backscattering modes only. More specialized variants of the technique are needed to probe forward-scattering modes. In this Brief Report, the symmetry of the phonon displacement field and the scattering line intensities have been analyzed for nonhigh-symmetry directions of the superlattices. For these purposes, we have explicitly included the full acoustic anisotropy in our calculations. We make quantitative comparison of the predictions with the measured frequencies of the quasi-LA (QLA) and quasi-(slow) TA (QSTA) modes, both of which have mixed LA and TA characteristics, and the pure (fast) TA (FTA) mode.

The SL samples used in the experiments were grown by molecular-beam epitaxy on semi-insulating (311) and (211) GaAs substrates. Both samples contained 40 period GaAs/AlAs SLs, and the initial design thicknesses of the layers were 28 monolayers (ML) of GaAs and 18 ML of AlAs. The samples were characterized postgrowth by x-ray diffraction and were found to be of excellent quality, and with layer thicknesses close to the design parameters. The period, d_{SL}, of the (311) sample was measured as 7.89 nm (made up from $d_{GaAs}=4.82$ nm of GaAs and $d_{AlAs}=3.07$ nm of AlAs), and the period of the (211) SL was measured as 8.24 nm (4.82 nm of GaAs and 3.42 nm of AlAs).

Measurements of the coherent SL phonons were made using a conventional reflection pump-probe technique: 100 fs, 10 nJ pulses from a mode-locked Ti:sapphire oscillator (repetition rate of 82 MHz) were split 90% to pump and 10% to probe. The pump beam was mechanically chopped at ~1 kHz and focused to a spot of diameter of about 100 μm on the sample which was mounted in an optical access cryostat. Allowing for the losses in the optical system, the pump fluence incident on the sample was 0.05 mJ cm^{-2}. The probe was passed through an optical delay and focused to a spot of about 50 μm diameter within the pump spot. The reflected probe was detected by a photodiode and lock-in amplifier using the pump chopper frequency as reference. All measurements were made with the sample at a temperature $T=12$ K in an optical cryostat. The laser wavelength was $\lambda_L=767$ nm, resonant with the fundamental gap of the SLs ($E1-HH1=1.62$ eV).

Figure 1(a) shows the change in probe reflectance (nor-

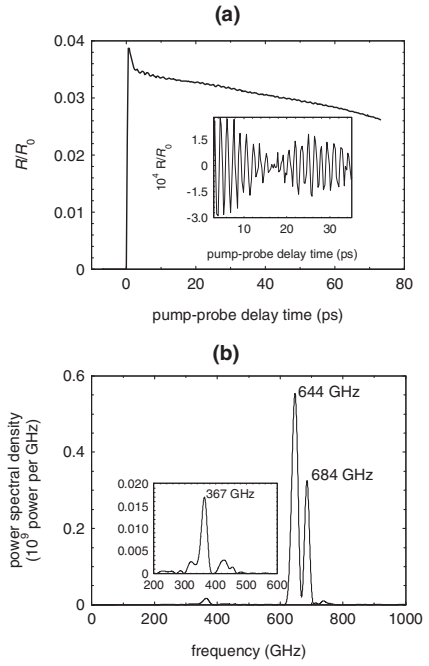

FIG. 1. (a) Probe reflectance as a function of the pump to probe delay time for the (311) GaAs/AlAs SL. The inset shows more closely the oscillations due to coherent phonons. (b) Fourier power spectrum of the pump-probe signal for the (311) SL. The inset shows the frequency range where the TA modes are observed.

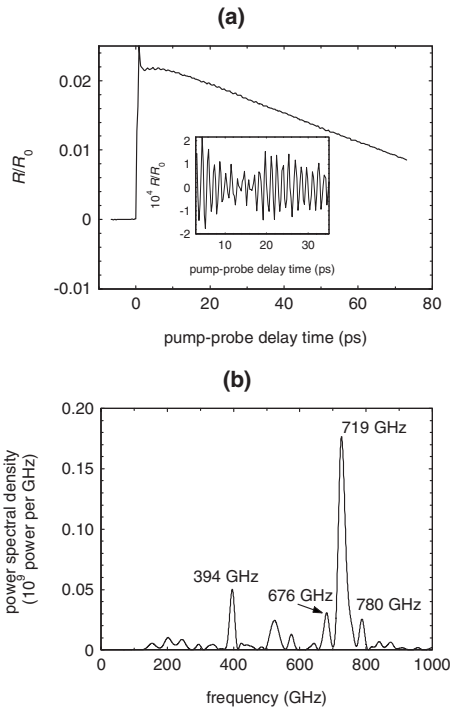

FIG. 2. (a) Probe reflectance as a function of the pump to probe delay time for the (211) GaAs/AlAs SL. The inset shows more closely the oscillations due to coherent phonons. (b) Fourier power spectrum of the pump-probe signal for the (211) SL.

malized to the background reflectance, R_0) as a function of the pump to probe time delay τ for the (311) sample. The usual step occurring at $\tau=0$ is due to the photoexcited carriers. Superimposed on the decay following the step, and shown more clearly in the inset, are the small ($R/R_0 \sim 10^{-4}$) oscillations due to the coherent SL phonons. In the Fourier power spectrum of the pump-probe signal, shown in Fig. 1(b), there are strong peaks at 643 and 684 GHz. The average speed of longitudinal sound in the (311) SL is: $c_s = d_{\mathrm{SL}}/(d_{\mathrm{GaAs}}/5.2 + d_{\mathrm{AlAs}}/6.2) \times 10^3$ ms^{-1} $= 5.5 \times 10^3$ ms^{-1}. Therefore $c_s/d_{\mathrm{SL}} \approx 697$ GHz, and, by comparison with previous work on (100) SLs,[3] it would seem reasonable at this stage to attribute the peaks to the QLA SL modes. A weaker series of peaks is observed in the region of 400 GHz [see inset of Fig. 1(b)]. Similar considerations to above lead us to attribute these to the QSTA and FTA SL modes. The pump-probe signal and corresponding Fourier power spectrum for the (211) sample are shown in Fig. 2. For this sample strong peaks corresponding to coherent QLA phonons are observed at frequencies of 676 and 719 GHz. Again, we can detect weak peaks in the region of 400 GHz due to the QSTA and FTA modes.

A more accurate determination of the mode frequencies for the (311) and (211) samples is made using the Fourier expansion method.[7] The Christoffel equation,

$$\rho(\mathbf{r})\ddot{u}_i - \sum_{jkl} \partial_j [C^{ijkl}(\mathbf{r})\partial_l u_k] = 0, \tag{1}$$

is written in terms of the Fourier series of the displacement $\mathbf{u}(\mathbf{r},t) = e^{-i\omega t}\Sigma_s \mathbf{u}_s(\mathbf{q}) e^{i(\mathbf{q}+s\mathbf{G})\mathbf{r}}$, elastic constants $C^{ijkl}(\mathbf{r}) = \Sigma_s C_s^{ijkl} e^{is\mathbf{Gr}}$, and mass density $\rho(\mathbf{r}) = \Sigma_s \rho_s e^{is\mathbf{Gr}}$. Here, $\mathbf{G} = \mathbf{e}_n 2\pi/d_{\mathrm{SL}}$, where $\mathbf{e}_n$ is the unit vector parallel to the SL growth direction. As a result we obtain for a given phonon wave vector $\mathbf{q}$ the Fourier components $\mathbf{u}_s^{(\mu,p)}(\mathbf{q})$ of the SL eigendisplacement modes classified by polarization μ and branch p (or frequency ω). The direction of the vectors $\mathbf{u}_s^{(\mu,p)}(\mathbf{q})$ determines also the phonon polarization vectors $\mathbf{e}_{\mu,\mathbf{q}}$. The calculated polarizations are shown in Table I. Clearly evident is the mixed longitudinal and transverse characteristics of the QSTA and QLA modes. In the case of the (311) SL the QLA and QSTA modes are, e.g., polarized along the [211] and [−111] directions, respectively, and not parallel to [311] and [2−3−3]. Figure 3 shows the frequencies, $f = \omega/2\pi$, of the SL phonons, with polarization μ and branch p, as a function of the wave vector $\mathbf{q}$ for the (311) SL.

Assuming that the folded acoustic phonon modes are impulsively generated due to Stokes scattering of the laser light, the number of the generated phonons will be proportional to the (Raman) light-scattering efficiency. Generalizing the approach of Colvard *et al.*[8] to arbitrary SL symmetry and arbitrary phonon propagation,

TABLE I. Polarizations of the phonon modes for (311) and (211) SL. Note that these are approximate for the cases of the QLA and QSTA modes.

Mode/SL orientation	(311) SL	(211) SL
QSTA	[−111]	[−433]
FTA	[01−1]	[01−1]
QLA	[211]	[322]

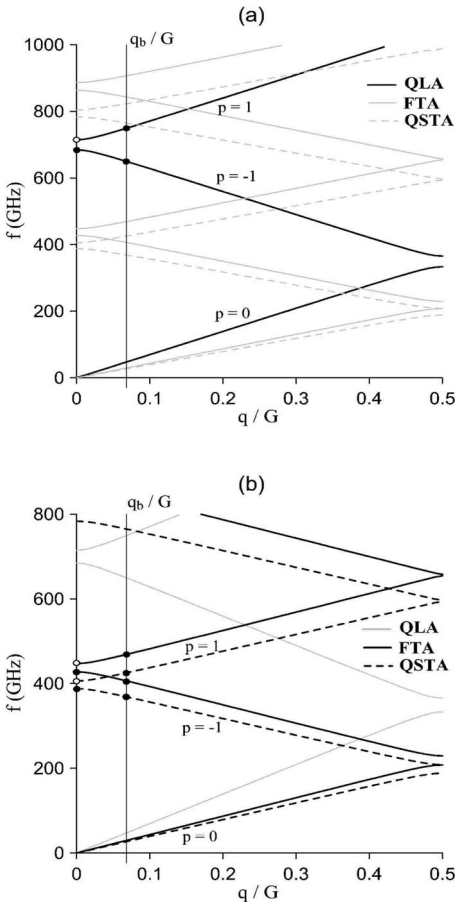

FIG. 3. Calculated phonon dispersion (all branches) for the (311) SL. The circles indicate possible modes involved in forward scattering ($q_f \approx 0$) and backscattering ($q_b = 4\pi n_{av}/\lambda_L$) for (a) the QLA and (b) the transverse polarizations. The open circles indicate modes that are predicted to be not active.

$$I \sim \left| \sum_s (q+sG) \left\{ p_{-s}^{44} \mathbf{e_q} (\mathbf{u}_s^{(\mu,p)} \mathbf{e}_L) + p_{-s}^{12} \mathbf{e}_L (\mathbf{u}_s^{(\mu,p)} \mathbf{e_q}) + p_{-s}^{xx} \sum_{i=1}^{3} \mathbf{e}_i (\mathbf{e_q})_i (\mathbf{u}_s^{(\mu,p)})_i (\mathbf{e}_L)_i \right\} \right|^2, \quad (2)$$

where $\mathbf{e_q}$ is the direction of the phonon wave vector (assumed parallel to $\mathbf{e}_n$), $\mathbf{e}_L$ is the polarization of the incident laser light (assumed perpendicular to $\mathbf{e}_n$), and the p_s^α are the Fourier components of the elements of the photoelastic tensor p^{44}, p^{12}, and $p^{xx} \equiv p^{11} - p^{12} - 2p^{44}$. Taking advantage of symmetry planes located in the middle of each SL layer, we choose the coordinate origin on the middle of a GaAs layer. Therefore, the Fourier components p_s^α corresponds to the coefficients of a square-wave function

$$p_s^\alpha = \begin{cases} \bar{p}^a & \text{for } s = 0 \\ \delta p^\alpha \dfrac{\sin(s\pi d_{\mathrm{GaAs}}/d_{\mathrm{SL}})}{s\pi} & \text{for } s \neq 0 \end{cases}, \quad (3)$$

with $\bar{p}^\alpha = (p^\alpha_{\mathrm{GaAs}} d_{\mathrm{GaAs}} + p^\alpha_{\mathrm{AlAs}} d_{\mathrm{AlAs}})/d_{\mathrm{SL}}$, $\delta p^\alpha = p^\alpha_{\mathrm{GaAs}} - p^\alpha_{\mathrm{AlAs}}$, and $\alpha = 11, 12, 44$.

Using Eq. (3) the scattering intensity can be written in the form

$$I \sim \left| \bar{p}^{44} \mathbf{e_q} (\tilde{\mathbf{u}}_0^{(\mu,p)} \mathbf{e}_L) + \bar{p}^{12} \mathbf{e}_L (\tilde{\mathbf{u}}_0^{(\mu,p)} \mathbf{e_q}) + \bar{p}^{xx} \sum_{i=1}^{3} \mathbf{e}_i (\mathbf{e_q})_i (\tilde{\mathbf{u}}_0^{(\mu,p)})_i (\mathbf{e}_L)_i + \delta p^{44} \mathbf{e_q} (\tilde{\mathbf{u}}^{(\mu,p)} \mathbf{e}_L) + \delta p^{12} \mathbf{e}_L (\tilde{\mathbf{u}}^{(\mu,p)} \mathbf{e_q}) + \delta p^{xx} \sum_{i=1}^{3} \mathbf{e}_i (\mathbf{e_q})_i (\tilde{\mathbf{u}}^{(\mu,p)})_i (\mathbf{e}_L)_i \right|^2, \quad (4)$$

where $\tilde{\mathbf{u}}_0^{(\mu,p)} = q \mathbf{u}_0^{(\mu,p)}(\mathbf{q})$ and

$$\tilde{\mathbf{u}}^{(\mu,p)} = \frac{q}{\pi} \sum_{s>0} \frac{\mathbf{u}_s^{(\mu,p)} + \mathbf{u}_{-s}^{(\mu,p)}}{s} \sin\left(\frac{\pi s d_{\mathrm{GaAs}}}{d_{\mathrm{SL}}}\right) + \frac{2}{d_{\mathrm{SL}}} \sum_{s>0} (\mathbf{u}_s^{(\mu,p)} - \mathbf{u}_{-s}^{(\mu,p)}) \sin\left(\frac{\pi s d_{\mathrm{GaAs}}}{d_{\mathrm{SL}}}\right).$$

Equation (4) generalizes former results[9] which were only valid for $q=0$ (i.e., for the case of phonon generation by forward scattering of light). For $q \approx 0$, Eq. (4) reduces to

$$I \sim \left| \left[\delta p^{44} \mathbf{e_q} (\mathbf{e}_{\mu,\mathbf{q}} \mathbf{e}_L) + \delta p^{12} (\mathbf{e}_{\mu,\mathbf{q}} \mathbf{e_q}) + \delta p^{xx} \sum_{i=1}^{3} \mathbf{e}_i (\mathbf{e_q})_i (\mathbf{e}_{\mu,\mathbf{q}})_i (\mathbf{e}_L)_i \right] \times \sum_{s>0} (\mathrm{u}_s^{(\mu,p)} - \mathrm{u}_{-s}^{(\mu,p)}) \sin\left(\frac{\pi s d_{\mathrm{GaAs}}}{d_{\mathrm{SL}}}\right) \right|^2. \quad (5)$$

For the considered symmetry, the main contribution to the sum over s in Eqs. (4) and (5) comes from the terms with $s=p$. For $q \approx 0$ our results for the Fourier components of the phonon modes show that practically only the terms $\mathrm{u}_s^{(\mu,p)}$ with $s = \pm p$ are nonzero. For q in the range of $2k_L$ (important for backscattering of light), the term with $s=p$ is the dominant one by approximately one order of magnitude.

Considering now phonon detection by the probe beam, the generated coherent phonon modes modulate the dielectric tensor and so change the reflectivity of the SL. In unstrained GaAs, the index ellipsoid is spherical, i.e., $n_1 = n_2 = n_3$ with $n_i = \varepsilon_i^{1/2}$, where ε_i are the principal dielectric constants. Deformation of the dielectric tensor by the phonons is due to the photoelastic effect

$$\Delta \varepsilon_{ij}^{-1} = \Delta \varepsilon_{i'} = \sum_{r'} p^{i'r'} S_{r'}, \quad (6)$$

where i' and r' (running from one to six) are the suppressed indices for the symmetric pairs (ij) and (rl), respectively, and $S_{r'}$ is the strain tensor. For the given crystal symmetry it follows also here that only the components $p_{11} = p_{22} = p_{33}$, $p_{12} = p_{13} = p_{21} = p_{23} = p_{31} = p_{32}$, and $p_{44} = p_{55} = p_{66}$ of the photoelastic tensor are different from zero. For normal incidence, the probe reflectance is given by

TABLE II. Frequencies of modes for (311) SL. The experimentally measured frequencies are in brackets and the error in these is ±3 GHz.

SL phonon modes	q_b; $p=-1$ (GHz)	q_f; $p=-1$ (GHz)	q_b; $p=+1$ (GHz)	q_f; p=+1 (GHz)
QSTA	368 (367)	388 (389)	425 (426)	406 (405)
FTA	406 (405)	428 (429)	469 (472)	447 (not present)
QLA	650 (644)	684 (684)	749 (741)	715 (710; weak)

$$R = \left| \frac{\tilde{n} - 1}{\tilde{n} + 1} \right|^2, \tag{7}$$

where $\tilde{n}=n+i\kappa$ is the complex refractive index. Therefore the change in reflectance

$$\Delta R = \left(\frac{\partial R}{\partial n} \right) \Delta n, \tag{8}$$

with $\Delta n = \Delta n(p^{11}, p^{12}, p^{44})$.

It follows that the reflectance measurement in the near-normal-incidence direction is sensitive to phonons with wave vector parallel to $\mathbf{e}_n$. Phonons with $q=q_f \approx 0$ (forward scattering of light) and $q=q_b=2k_L=4\pi n_{av}/\lambda_L$ (backward scattering) are probed. Tables II and III compare the calculated and the experimentally measured phonon frequencies for all modes. Because the TA signal was close to the noise floor, a statistical analysis of about 20 experimental runs was used to identify the peaks in the experimental data. Excellent agreement of the frequencies is obtained for the (311) SL using the measured SL parameters; in the case of the (211) SL, it was necessary to make a small correction to the GaAs and AlAs layer thicknesses to obtain good agreement of the frequencies. This is reasonable in view of the difficulty in obtaining accurate x-ray results for this wafer orientation.

We now consider the relative strengths of the detected modes. It is difficult to obtain reliable theoretical predictions for the intensities due to uncertainty in the values of the photoelastic tensor for GaAs and AlAs, particularly for wavelengths close to an optical resonance. However, we can reach some qualitative conclusions based on comparison of the model predictions with the measurements. The calculated Fourier components of the displacement vector $\mathbf{u}_s^{(\mu,p)}(\mathbf{q})$ are, for polarization, μ(=QLA,QSTA,FTA) and $q \approx 0$, symmetric with respect to the midplane of a layer for $p=+1$ (i.e., $\mathbf{u}_s^{(\mu,+1)}=\mathbf{u}_{-s}^{(\mu,+1)}$) and antisymmetric for $p=-1$. Therefore, from the above Eq. (5) for the light-scattering efficiency, it is clear that the (symmetric) mode with $p=+1$ should be not active in forward scattering. This is clearly the case for the (211) SL. However, for the (311) SL, the symmetric QSTA and QLA modes due to forward scattering are detected, albeit weakly. This could be due to a small amount of disorder in the SL resulting in relaxing of the selection rules for Raman scattering. As already mentioned, for backscattering, the Fourier components $u_s^{(\mu,p)}$ are nonzero only for $s=p$. Our theoretical calculations suggest that the higher intensity is obtained for the mode with $p=-1$, and this appears consistent with the measurements. It is also interesting to note that, for the QLA modes, the backscattering signal is stronger than that due to forward scattering. This is in contrast to what is normally seen with (100) SLs where the forward-scattering peak is dominant.

TABLE III. Frequencies of modes for (211) SL. Calculations were for the SL period consisting of 26 ML GaAs and 20 ML AlAs. The experimentally measured frequencies are in brackets and the error in these is ±3 GHz.

SL phonon modes	q_b; $p=-1$ (GHz)	q_f; $p=-1$ (GHz)	q_b; $p=+1$ (GHz)	q_f; $p=+1$ (GHz)
QSTA	350 (354)	370 (372)	403 (not present)	383 (not present)
FTA	394 (394)	416 (414)	453 (450)	431 (not present)
QLA	676 (676)	715 (719)	778 (780)	739 (not present)

In summary, we have generated terahertz coherent phonons in low-symmetry GaAs/AlAs SLs by femtosecond optical pumping and detected them by measuring the reflectance of time delayed, femtosecond probe pulses. Good agreement between the observed and calculated mode frequencies was obtained for both (311) and (211) SLs, which supports the initial assumption used in the calculations that Raman scattering is responsible for the phonon generation. Quantitative modeling of the observed intensities will require more information about the values of the photoelastic tensor elements for GaAs and AlAs.

The authors would like to thank C. R. Staddon for providing the x-ray characterization data.

[1] A. Yamamoto *et al.*, Phys. Rev. Lett. **73**, 740 (1994).
[2] A. Bartels *et al.*, Phys. Rev. Lett. **82**, 1044 (1999).
[3] N. M. Stanton *et al.*, Phys. Rev. B **68**, 113302 (2003).
[4] R. N. Kini *et al.*, Appl. Phys. Lett. **88**, 134112 (2006).
[5] Z. V. Popović *et al.*, Phys. Rev. B **48**, 1659 (1993).
[6] Z. V. Popović *et al.*, Superlattices Microstruct. **14**, 173 (1993).
[7] Y. Tanaka *et al.*, J. Phys.: Condens. Matter **10**, 8787 (1998).
[8] C. Colvard *et al.*, Phys. Rev. B **31**, 2080 (1985).
[9] E. Anastassakis and Z. V. Popovic, J. Raman Spectrosc. **27**, 207 (1996).